Uncertainty Quantification of the Modal Rotation Shape Sensing Method for Geometrically Non-Linear Deformation

Janto Gundlach [1]*, Marc Böswald* [2]*, Martin Tang* [3]*, and Jurij Sodja* [4]

[1] German Aerospace Center, Institute of Aeroelasticity, Bunsenstraße 10, 37085 Göttingen, Germany, *janto.gundlach@dlr.de*

[2] German Aerospace Center, Institute of Aeroelasticity, Bunsenstraße 10, 37085 Göttingen, Germany, *marc.boeswald@dlr.de*

[3] German Aerospace Center, Institute of Aeroelasticity, Bunsenstraße 10, 37085 Göttingen, Germany, *martin.tang@dlr.de*

[4] Delft University of Technology, Kluyverweg 1, 2629HS Delft, The Netherlands, *j.sodja@tudelft.nl*

ABSTRACT

There are technical applications where structures undergo deformation in the geometrically non-linear domain. This is the case for high-aspect-ratio wings, which may play a more important role in the future aircraft designs. Shape sensing methods can estimate the deflection of these structures during operation, if a direct measurement of the displacements is inconvenient or not possible. For the geometrically non-linear range, the modal rotation method has been proposed as a candidate suitable for slender structures. The method superposes modal rotation increments of segments along the length of the structure, typically obtained from a finite element model. If the method is applied model-free, based on modal rotations identified from test data, the variability of the modal rotations leads to uncertainty in the displacement estimates. The present study illustrates how displacement output uncertainty can be expressed using linearised propagation formulae, relying on the prerequisite that the modal rotations exhibit a normally distributed and independent scatter around their mean. This uncertainty propagation is investigated in the shape sensing of a high-aspect-ratio wing model, and verification through Monte Carlo simulations demonstrates that the derived expressions accurately propagate the uncertainty from variable modal rotations. Consequently, these expressions can be applied to specific shape sensing tasks in experiments where this variability can be recorded.

Keywords: Shape Sensing, Modal Rotations, Modal Approach, Uncertainty Quantification

1. INTRODUCTION

In response to the growing demand for more sustainable and eco-friendly aviation, high aspect-ratio wings are considered in future aircraft designs to reduce induced drag [1]. Such wings are more sus-

ceptible to large deflections, their aeroelastic behavior is prone to being influenced by geometric non-linearities which affects their aeroelastic behaviour. The non-linearities are of particular interest from a structural dynamics perspective, since they lead to changes in modal parameters, which in turn directly affect the aeroelastic stability of associated structures. In order to discern whether the change in modal properties is due to geometric non-linearities or a change in flow conditions, continuous monitoring of wing deflections, along with other values such as dynamic pressure, is necessary during a wind tunnel test or flight. The displacement reconstruction of wing-like structures based on strain or other kinematic quantities, commonly denoted as shape sensing [2], is a prospective method for monitoring the state of deflection whenever a direct measurement is not feasible. Different approaches for estimating the displacements in the geometrically non-linear range have been proposed, where the non-linearity is captured in an incremental sense [3, 4]. The modal rotations method (MRM) [5], on the other hand, estimates non-linear displacements in a single step, which is accomplished by linear superposition of modal rotations of the undeformed structure on a reference line. In the process, the rotation mode shapes are obtained by normal modes analysis of the finite element model of the structure. The modal approach using mode shapes of rotation increments is considered accurate, as the absolute rotation increments remain small even in case of large deflections of the slender structure. In principle, modal rotations can be identified in experimental or operational modal analysis, for instance, using data obtained with gyroscopic sensors. Steady progress in the field of MEMS measuring rates of rotation make these sensor types more prospective for application [6]. In [7] ground test results and mode tracking during flight demonstrate the applicability of such sensors for modal identification. However, significant noise in the signals requires long measurement times to improve particularly the damping estimates. If MRM is used model-free and rotation mode shapes from test data are used in the shape sensing, the displacement reconstruction will be affected by the uncertainties which are inevitably present in the identification results. For this purpose, in this study linearised Gaussian propagation is employed to derive analytical expressions to assess the output uncertainty of individual displacement components.

2. THEORY

The method introduced in [5] can be applied to 3D cases. As the focus of this work lies on the uncertainty properties of MRM, the 2D version of the method is considered in the following. On that account, only the uncertainties concerning flapwise bending deformation of a wing structure are investigated. For application on more complex 3D problems, the uncertainty analysis has to be extended.

2.1. Modal rotations method

It is assumed that the modal rotations are identified along a spanwise reference line of the structure which is defined in the yz-plane. As depicted in Figure 1, the structure is discretised in N_s segments.
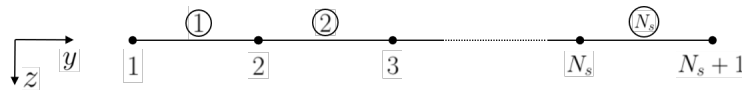

Figure 1: Segments and nodes describing an arbitrary reference line of the slender structure.

Modal rotations $\phi_{\theta_m^{(i)}}$ of $m = 1, \ldots, N_m$ modes are determined at the $i = 1, \ldots, N_s + 1$ nodal positions. For each segment, a modal rotation increment can be defined using the modal rotations at the nodal points:

$$\Delta\phi_{\theta_{sm}} = \phi_{\theta_m^{(s+1)}} - \phi_{\theta_m^{(s)}}. \tag{1}$$

These can be stored in a matrix containing modal rotation increments for all modes and segments:

$$\boldsymbol{\Delta\Phi}_\theta = \begin{bmatrix} \Delta\phi_{\theta_{11}} & \cdots & \Delta\phi_{\theta_{1N_m}} \\ \vdots & & \vdots \\ \Delta\phi_{\theta_{N_s1}} & \cdots & \Delta\phi_{\theta_{N_sN_m}} \end{bmatrix}. \tag{2}$$

A key aspect of MRM is that the rotation increments along the structure are computed in terms of the modal superposition

$$\Delta\boldsymbol{\theta} = \Delta\boldsymbol{\Phi}_\theta\boldsymbol{q} \tag{3}$$

with the modal coordinates $\boldsymbol{q}$ being the coefficients of the linear combination. The modal coordinates can be determined in different ways. With known external forces and generalised stiffnesses, they are obtainable from equilibrium in modal space (cf. [5]), otherwise $\boldsymbol{q}$ can be determined by linear regression of strain mode shapes on strain values (cf. [4]). If determined solely from measured data, additional uncertainty in the modal coordinates has to be taken into account, which is not dealt with in this study. The rotation increments of the segments are employed in rotation matrices

$$\boldsymbol{R}_s = \boldsymbol{R}_{s-1}\boldsymbol{\Delta R}_s; \quad \boldsymbol{\Delta R}_s = \begin{bmatrix} \cos\Delta\theta_s & -\sin\Delta\theta_s \\ \sin\Delta\theta_s & \cos\Delta\theta_s \end{bmatrix}, \quad s = 1,\ldots,N_s \tag{4}$$

to compute the location of the nodes $\boldsymbol{x}^{(i)} = [y^{(i)},\, z^{(i)}]^T$ in the deformed states, starting from the root outboard to the tip

$$\boldsymbol{x}^{(i)} = \boldsymbol{x}^{(i-1)} + \boldsymbol{R}_{i-1}\boldsymbol{\Delta l}_{i-1}, \quad i = 2,\ldots,N_s+1, \tag{5}$$

where $\boldsymbol{\Delta l}_{i-1} = \boldsymbol{X}^{(i)} - \boldsymbol{X}^{(i-1)}$ describes the length vector of the $(i-1)$-th segment in the undeformed configuration. The estimated displacement vector of the i-th node is computed as

$$\hat{\boldsymbol{u}}^{(i)} = \boldsymbol{x}^{(i)} - \boldsymbol{X}^{(i)}. \tag{6}$$

2.2. Uncertainties from modal rotations

In order to assess the impact of possible uncertainties in identified modal rotations, it is assumed that nodal components of each mode shape vector scatters around the mean μ_{θ_m} with a normal distribution characterised by the standard deviation σ_{θ_m}. It is furthermore assumed that the modal rotations and associated uncertainties are independent from each other. With these assumptions, the Gaussian error propagation formula is applicable to evaluate the uncertainty in the displacement output. In general, the uncertainty for the displacement components at i-th node reads:

$$\sigma_{\hat{\boldsymbol{u}}_{y/z}^{(i)}} = \sqrt{\sum_{m=1}^{N_m}\sum_{j=1}^{N_s+1}\left(\left(\frac{\partial\hat{\boldsymbol{u}}^{(i)}}{\partial\phi_{\theta_m}^{(j)}}\right)_{y/z}\sigma_{\theta_m^{(j)}}\right)^2}. \tag{7}$$

To gain insight into the partial derivatives in the expression, they are broken down step by step. From Eq. (6) only the nodal coordinates $\boldsymbol{x}^{(i)}$ of the deformed states that depend on $\phi_{\theta_m}^{(j)}$, which, according to Eqs. (1-4), are isolated in the incremental rotation matrices. Therefore, the recursive formulation of the nodal positions in Eq. (5) is expressed from the root outboard by means of rotation matrix increments:

$$\boldsymbol{x}^{(i)} = \boldsymbol{x}^{(1)} + \sum_{k=1}^{i-1}\left(\prod_{j=1}^{k}\boldsymbol{\Delta R}_j\right)\boldsymbol{\Delta l}_k, \quad i = 2,\ldots,N_s+1. \tag{8}$$

For the node located at the root, it is assumed that the position in the deformed states is known, e.g. $\boldsymbol{x}^{(1)} = \boldsymbol{X}^{(1)}$ if the root is rigidly clamped. Considering the remaining nodes, the product rule implies the derivation with respect to the modal rotation of the m-th mode at the j-th node:

$$\frac{\partial\boldsymbol{x}^{(i)}}{\partial\phi_{\theta_m}^{(j)}} = \sum_{k=1}^{i-1}\left(\sum_{n=1}^{k}\left(\prod_{p=1}^{n-1}\boldsymbol{\Delta R}_p\right)\frac{\partial\boldsymbol{\Delta R}_p}{\partial\phi_{\theta_m}^{(j)}}\left(\prod_{q=p+1}^{k}\boldsymbol{\Delta R}_q\right)\right)\boldsymbol{\Delta l}_k. \quad j = 1,\ldots,i. \tag{9}$$

Note that in the expression the empty product convention is used, which indicates multiplication with unity if no elements are in the product. With view on Eqs. (8) and (1-4), one observes that only derivatives with respect to modal rotations of the first i nodes are defined. For a clamped structure, the number of derivatives is reduced by the number of derivatives with respect to $\phi_{\theta_m^{(1)}}$. The number of terms in Eq. (9) is significantly reduced with further insight into the derivatives of the incremental rotation matrices. These only exist for incremental rotations of the $(j-1)$-th and j-th segment, respectively, such that the updated equation yields

$$
\frac{\partial \boldsymbol{x}^{(i)}}{\partial \phi_{\theta_m^{(j)}}} = \sum_{k=j-1}^{i-1} \left(\prod_{p=1}^{j-2} \boldsymbol{\Delta R}_p \right) \frac{\partial \boldsymbol{\Delta R}_{j-1}}{\partial \phi_{\theta_m^{(j)}}} \left(\prod_{q=j}^{k} \boldsymbol{\Delta R}_q \right) \boldsymbol{\Delta l}_k
$$
$$
+ \sum_{k=j}^{i-1} \left(\prod_{p=1}^{j-1} \boldsymbol{\Delta R}_p \right) \frac{\partial \boldsymbol{\Delta R}_{j}}{\partial \phi_{\theta_m^{(j)}}} \left(\prod_{q=j+1}^{k} \boldsymbol{\Delta R}_q \right) \boldsymbol{\Delta l}_k.
\tag{10}
$$

By definition of Eq. (4) and recalling that the rotation increment of each segment is obtained from linear superposition (cf. Eq. (3)), the remaining derivatives are computed via

$$
\frac{\partial \boldsymbol{\Delta R}_{j-1}}{\partial \phi_{\theta_m^{(j)}}} = q_m \begin{bmatrix} -\sin \Delta\theta_{j-1} & -\cos \Delta\theta_{j-1} \\ \cos \Delta\theta_{j-1} & -\sin \Delta\theta_{j-1} \end{bmatrix} \quad \text{and} \quad \frac{\partial \boldsymbol{\Delta R}_{j}}{\partial \phi_{\theta_m^{(j)}}} = -q_m \begin{bmatrix} -\sin \Delta\theta_j & -\cos \Delta\theta_j \\ \cos \Delta\theta_j & -\sin \Delta\theta_j \end{bmatrix}.
\tag{11}
$$

From these results it is apparent that the derivatives can directly be expressed by a rotation of the incremental rotation matrices about 90°:

$$
\frac{\partial \boldsymbol{\Delta R}_{j-1}}{\partial \phi_{\theta_m^{(j)}}} = q_m \boldsymbol{R}_{\frac{\pi}{2}} \boldsymbol{\Delta R}_{j-1} \quad \text{and} \quad \frac{\partial \boldsymbol{\Delta R}_{j}}{\partial \phi_{\theta_m^{(j)}}} = -q_m \boldsymbol{R}_{\frac{\pi}{2}} \boldsymbol{\Delta R}_{j} \quad \text{with} \quad \boldsymbol{R}_{\frac{\pi}{2}} = \begin{bmatrix} 0 & -1 \\ 1 & 0 \end{bmatrix}.
\tag{12}
$$

A rotation by 90° is a special case, since the rotation is commutative with other rotation matrices. For this reason, the respective rotation matrix can be factorised outside of the summation and Eq. (10) is further simplified to

$$
\frac{\partial \boldsymbol{x}^{(i)}}{\partial \phi_{\theta_m^{(j)}}} = q_m \boldsymbol{R}_{\frac{\pi}{2}} \left[\sum_{k=j-1}^{i-1} \left(\prod_{p=1}^{j-2} \boldsymbol{\Delta R}_p \right) \boldsymbol{\Delta R}_{j-1} \left(\prod_{q=j}^{k} \boldsymbol{\Delta R}_q \right) \boldsymbol{\Delta l}_k \right.
$$
$$
\left. - \sum_{k=j}^{i-1} \left(\prod_{p=1}^{j-1} \boldsymbol{\Delta R}_p \right) \boldsymbol{\Delta R}_{j} \left(\prod_{q=j+1}^{k} \boldsymbol{\Delta R}_q \right) \boldsymbol{\Delta l}_k \right].
\tag{13}
$$

Since $\boldsymbol{\Delta R}_0$ is not defined, the first summation vanishes for all derivatives with respect to $\phi_{\theta_m^{(1)}}$. For all other derivatives with $j \in [2, i]$, the terms in the first summation coincide with terms in the second summation except for the very first term where $k = j - 1$. Therefore, the displacement sensitivities are finally computable via

$$
\frac{\partial \hat{\boldsymbol{u}}^{(i)}}{\partial \phi_{\theta_m^{(j)}}} = \frac{\partial \boldsymbol{x}^{(i)}}{\partial \phi_{\theta_m^{(j)}}} = \begin{cases} -q_m \boldsymbol{R}_{\frac{\pi}{2}} \sum_{k=1}^{i-1} \boldsymbol{\Delta R}_1 \left(\prod_{q=2}^{k} \boldsymbol{\Delta R}_q \right) \boldsymbol{\Delta l}_k, & \text{if} \quad j = 1 \\ q_m \boldsymbol{R}_{\frac{\pi}{2}} \left(\prod_{p=1}^{j-1} \boldsymbol{\Delta R}_p \right) \boldsymbol{\Delta l}_{j-1}, & \text{if} \quad 2 \le j \le i. \end{cases}
\tag{14}
$$

The uncertainty propagation formula requires scalar sensitivities for each coordinate direction. Therefore, the vectorial terms are multiplied with $\boldsymbol{R}_{\frac{\pi}{2}}$. The multiplication exhibits the property $\boldsymbol{R}_{\frac{\pi}{2}} \boldsymbol{a} =$

$[-a_2, a_1]^T$ such that the scalar sensitivities crystallise in

$$
\left(\frac{\partial \hat{\boldsymbol{u}}^{(i)}}{\partial \phi_{\theta_m^{(j)}}}\right)_{y/z} = \begin{cases} \pm q_m \left\{ \displaystyle\sum_{k=1}^{i-1} \boldsymbol{\Delta R}_1 \left(\prod_{q=2}^{k} \boldsymbol{\Delta R}_q\right) \boldsymbol{\Delta l}_k \right\}_{z/y}, & \text{if } j = 1 \\[2em] \mp q_m \left\{ \left(\displaystyle\prod_{p=1}^{j-1} \boldsymbol{\Delta R}_p\right) \boldsymbol{\Delta l}_{j-1} \right\}_{z/y}, & \text{if } 2 \leq j \leq i. \end{cases} \tag{15}
$$

Due to the quadrature in Eq. (7), the opposing signs cancel each other out, resulting in the following uncertainty of the displacement output:

$$
\sigma_{\hat{\boldsymbol{u}}_{y/z}^{(i)}} = \left\{ \sum_{m=1}^{N_m} q_m^2 \left[\left(\left\{ \sum_{k=1}^{i-1} \boldsymbol{\Delta R}_1 \left(\prod_{q=2}^{k} \boldsymbol{\Delta R}_q\right) \boldsymbol{\Delta l}_k \right\}_{z/y} \sigma_{\theta_m^{(1)}} \right)^2 \right. \right.
$$
$$
\left. \left. + \sum_{j=2}^{i} \left(\left\{ \left(\prod_{p=1}^{j-1} \boldsymbol{\Delta R}_p\right) \boldsymbol{\Delta l}_{j-1} \right\}_{z/y} \sigma_{\theta_m^{(j)}} \right)^2 \right] \right\}^{\frac{1}{2}}. \tag{16}
$$

In case of a clamped cantilever structure and thus $\sigma_{\theta_m^{(1)}} = 0$, the first term cancels out for each mode in the sum. It is also apparent from the propagation formulae that the output uncertainty increases with increasing number of considered nodes and therefore sensors, if the method is applied on test data.

3. APPLICATION CASE

The uncertainty analysis of MRM is applied to the FE model of a high-aspect-ratio wing with symmetric cross-sections. The wing has a swept and tapered design, which typically leads to less accurate shape sensing estimates. Before uncertainties are considered in the modal rotations, the deterministic results of the method for a bending load case in the geometrically non-linear domain are presented. The wing model is composed of shells and shear webs made from sandwich-structured composites, along with ribs that reinforce the cross-sections at regular intervals. The geometric dimensions are provided in Tab. 1. The model consists primarily of 4-noded shell quadrilaterals with composite properties defining the laminate lay-up. It has been generated using the DLR-AE in-house parametric tool ModGen [8] in MSC.NASTRAN. A top view of the model is shown in Fig. 2. Since the wing is designed for multiple purposes, it includes a folding wingtip, which is not relevant to this study.

Table 1: Parameters of the wing geometry.

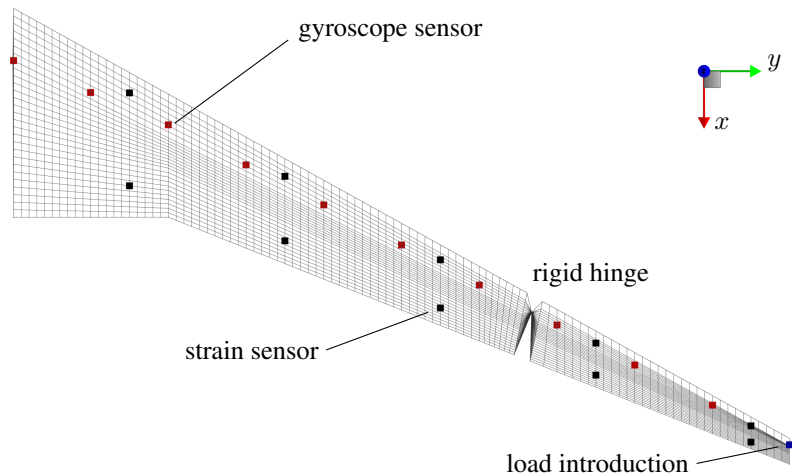| Parameter	Value
half span	$5\,\text{m}$
planform area	$3\,\text{m}^2$
aspect ratio	16.67
sweep angle	29°

Figure 2: Finite element grid of the wing with virtual gyroscope sensor and strain sensor positions.

The hinge of the wingtip is modelled as locked using RBE2 elements; it appears as a 0.1 m gap at two-thirds of the wing span. To conduct the shape sensing, it is assumed that modal rotations of $N_m = 10$ modes around the x-direction are available at 11 nodes (e.g. from gyroscope sensors) positioned equidistantly on the quarter chord line of the wing. Thus, the rotation of $N_s = 10$ segments is considered for the displacement estimate. The geometrically non-linear deformation is caused by a tip load in z-direction also acting at the quarter chord of the cross-section. In order to determine the linear coefficients required for the modal approach (Eq. (3)), it is assumed that the wing is instrumented with 20 strain sensors located on the panels on both the pressure and the suction sides. The sensors measure uniaxial strain in the deformed state and provide strain mode shape components of the first ten modes to compute the modal coordinates (cf. [4]). The deformation estimate using MRM for the described setting is
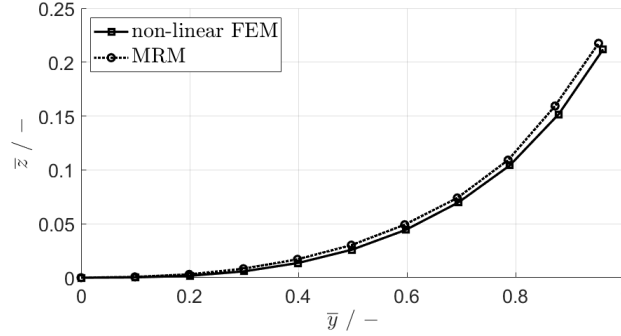

Figure 3: Deflection line estimate of MRM application in comparison with non-linear FEM results in coordinates normalised to the wing length.

depicted in Fig. 3, where the non-linear static FEM curve is considered as the true deformation result. If MRM was run model-free, uncertainties would affect the displacement output and the deterministic result would represent the mean displacement estimate.

4.   UNCERTAINTY QUANTIFICATION

In the following, Eq. (16) is evaluated with given normally distributed variability of the modal rotations. This is done by scaling the standard deviation of the modal rotation of each mode at every node to the deterministic value obtained from the FE model:

$$c_v^{\phi\theta} = \frac{\sigma_{\theta_m^{(i)}}}{\phi_{\theta_m}^{(i)}}. \tag{17}$$

According to this definition, every component of the modal rotation matrix is altered with the same coefficient of variation. However, if the variability of the modal rotations is known from experimental testing, they could still be taken into account individually. In theory, the displacement uncertainties can also be assessed using Monte Carlo simulations (MCS). However, this requires significant effort when a large number of nodes and samples are involved. In this study MCS is employed to verify the propagation formulae for MRM. Therefore, modal rotation matrices are sampled using Latin Hypercube Sampling in the UQLab framework [9]. The histograms in Fig. 4 illustrate the absolute frequency distribution of the nodal displacement $\boldsymbol{u}^{(11)}$ of the wing tip estimated by MRM in a MCS. In this simulation 10^6 modal rotation matrices of ten modes have been considered with $c_v^{\phi\theta} = 0.1$. The mean value and the standard deviation from the MCS results is provided next to the deterministic MRM estimate and the standard deviation of the output according to Eq. (16). For the displacements in both coordinate directions, the uncertainty from MCS coincides well with the analytical results. The absolute uncertainties in the flap-wise displacement estimates are higher than those in the spanwise displacement estimates, whereas the opposite is true for relative uncertainty. Regarding the MCS mean value, there is a small deviation to the deterministic reference of MRM, meaning that the distribution in the histogram is slightly asymmetrical, which is attributed to the non-linearity of the transformation from modal rotations to displacements in the
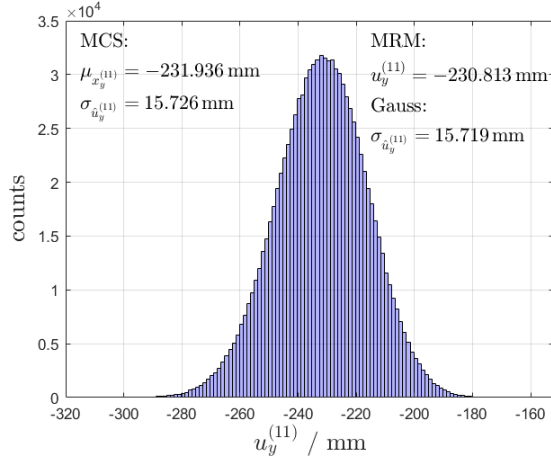
(a) Histogram of tip node location in y-direction.
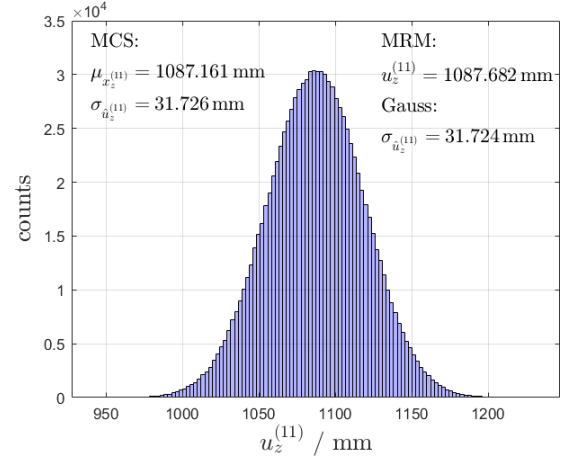
(b) Histogram of tip node location in z-direction.

Figure 4: Results from MCS using 10^6 sampled modal rotation matrices consisting of ten modes with $10\,\%$ coefficient of variation.

MRM procedure, where trigonometric functions are applied in the rotation matrices (cf. Eq. (4)). In fact, for smaller coefficients of variation, both the standard deviation and the mean value exhibit improved agreement to the deterministic MRM results in combination with Gaussian uncertainty propagation.
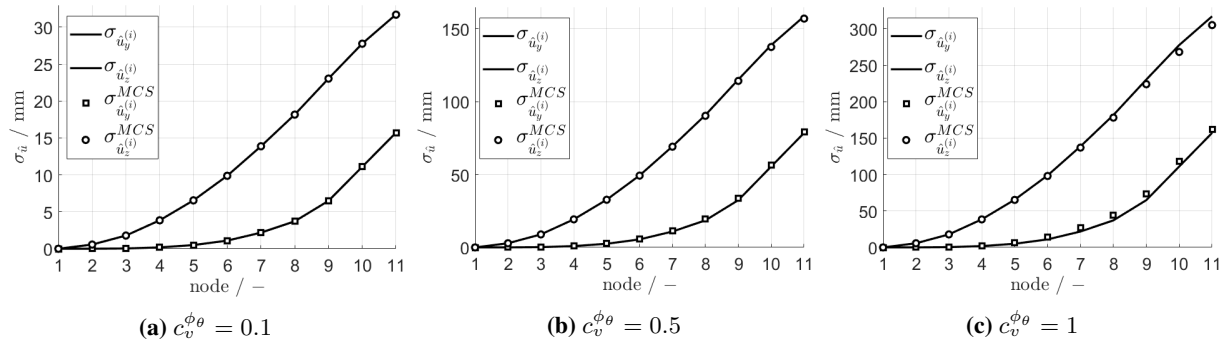

(a) $c_v^{\phi\theta} = 0.1$

(b) $c_v^{\phi\theta} = 0.5$

(c) $c_v^{\phi\theta} = 1$

Figure 5: Standard deviation of displacement estimates over nodes: Comparison of Eq. (16) with MCS for different coefficients of variation.

In Fig. 5, the displacement uncertainties in the two coordinate directions are shown for all nodes along the reference line. To facilitate comparison between the MCS and analytical uncertainties, different coefficients of variation are applied to scale the variability of the modal rotations. One recognises in the presented range of $c_v^{\phi\theta} = 0.1 - 1$ that the output uncertainties are proportional to the input standard deviation. Also, for both displacement directions, the uncertainty grows monotonously with increasing number of nodes along the reference line. Both properties can also be recognised from the structure of Eq. (16). As indicated in Fig. 5a, for $c_v^{\phi\theta} = 0.1$ the different results lie directly on top of each other. For $c_v^{\phi\theta} = 0.5$, the curves are still nearly indistinguishable. However, for $c_v^{\phi\theta} = 1$, where the standard deviation equals the mean value of the modal rotation, the MCS results show a noticeable deviation from the analytical results. This illustrates, in terms of uncertainty, very large coefficients of variation are necessary for the non-linearity to be expressed. These observations confirm that for reasonably low variability of the employed modal rotation modes, the propagation formulae can be used as a replacement for costly MCS to quantify the displacement uncertainty.

5. CONCLUSIONS

In this research, analytical uncertainty propagation formulae for the modal rotation method (MRM) have been presented. The shape sensing method has been applied on data provided by an FE model of a high-aspect-ratio wing with virtual instrumentation which is reasonable for a real wind tunnel test in terms of number and positions of sensors. The model is evaluated in a geometrically non-linear deformation state, where the uncertainty quantification analysis reveals that displacement uncertainty is proportional to the coefficient of variation of the modal rotation. Furthermore, the uncertainty grows from the root outboard with increasing node number. Finally, it was demonstrated that the analytical approach may replace an assessment via Monte Carlo simulations. Hence, the analytical quantification can contribute to the effective assessment of the quality of shape sensing with MRM within a complex measurement task in the geometrically non-linear domain.

REFERENCES

[1] Y. Ma and A. Elham. Designing high aspect ratio wings: A review of concepts and approaches. *Progress in Aerospace Sciences*, 145(100983), 2024. doi: 10.1016/j.paerosci.2024.100983.

[2] M. Gherlone, P. Cerracchio, and M. Mattone. Shape sensing methods: Review and experimental comparison on a wing-shaped plate. *Progress in Aerospace Science*, 99:14–26, 2018. doi: 10.1016/j.paerosci.2018.04.001.

[3] A. Tessler, R. Roy, M. Esposito, C. Surace, and M. Gherlone. Shape sensing of plate and shell structures undergoing large displacements using the inverse finite element method. *Shock and Vibration*, 2018. doi: 10.1155/2018/8076085.

[4] J. Gundlach, M. Böswald, and J. Sodja. An incremental modal shape sensing method for geometrically non-linear deformed wings. In *International Forum on Aeroelasticity and Structural Dynamics IFASD*, The Hague, The Netherlands, 2024.

[5] A. Drachinsky and D. E. Raveh. Modal rotations: A modal-based method for large structural deformations of slender bodies. *AIAA Journal*, 58(7):3159–3173, 2020. doi: 10.2514/1.j058899.

[6] Wenyi Huang, Xing Yan, Sengyu Zhang, Zhe Li, Jamal N. A. Hassan, Dingwei Chen, Guangjun Wen, Kai Chen, Deng Guangwei, and Yongjun Huang. Mems and moems gyroscopes: A review. *Photonic Sensors*, 13(4), 2023.

[7] M. Tang, K. Soal, M. Böswal, and Y. Govers. Application of gyroscopes for stability monitoring in flutter tests. In *Proc. 11th International Operational Modal Analysis Conference*, Rennes, France, 2025.

[8] T. Klimmek. Parameterization of topology and geometry for the multidisciplinary optimization of wing structures. In *Proceedings of the European Air and Space Conference 2009*, Manchester, UK, 2009.

[9] S. Marelli and B. Sudret. UQLab: A framework for uncertainty quantification in MATLAB. In: *The 2nd Internation Conference on Vulnerability and Risk Analysis and Management (ICVRAM 2014)*, 2014.